

Self-Assembling Chiral Gelators for Fluorinated Media[†]Marie Côté, Tim Nicholls, David W. Knight, Ian R. Morgan, Philippe G. A. Rogueda,[‡]
Stephen M. King, Richard K. Heenan, and Peter C. Griffiths*

School of Chemistry, Cardiff University, Main Building, Park Place, Cardiff CF10 3AT, U.K.
[‡] *Formerly at AstraZeneca Research and Development, Charnwood, Bakewell Road, Loughborough
LH11 5RH, U.K.*

Received December 31, 2008. Revised Manuscript Received March 19, 2009

Formulations involving partially and fully fluorinated media represent a technological challenge given the lipophobic and hydrophobic nature of such liquids. The identification of self-associating materials with which to control the viscosity and solubilizing characteristics of fluorinated solvents is a particularly interesting area of research. It is shown here that the presence of the stereogenic centers inherent in a family of *bis*-(α,β -dihydroxy ester)s is an essential requirement for the thermoreversible gelation of mixtures of partially fluorinated liquids 2*H*,3*H*-perfluoropentane (HPFP) and 1*H*,1*H*-heptafluorobutanol (HFB). Gelation is driven by hydrogen bonding, which induces a nonpreferred conformation around the *bis*-(α,β -dihydroxy ester) structural motif. An analysis of the melting temperature yields an enthalpy of melting that is consistent with three to four hydrogen bonds, commensurate with the end-group structure of the gelator. Small-angle neutron scattering demonstrated the existence of the common fibrillar structures whose dimensions showed no obvious correlation with the molecular structure of the gelator.

Introduction

The spontaneous self-assembly and network formation of low-molecular-mass organogelators (LMOGS) has stimulated much research attempting to quantify the fundamental aspects of this fascinating phenomenon.^{1–5} However, whereas a number of structurally diverse gelators have been identified, it is not yet possible to design a gelator a priori for a selected liquid.^{3–15}

Gelation by LMOGS is clearly not driven by a single molecular interaction because a range of physical (noncovalent) interactions, principally hydrogen bonding but also solvophobic effects or π – π interactions, play a role. Recently, for example,

Berkhardt et al.¹⁶ have studied the gelation of a range of organic solvents by 12-hydroxy stearic acid (HAS) in the presence of added alcohol, which is known to disrupt hydrogen bonds. At sufficiently high levels of added alcohol, gelation was precluded, suggesting a hydrogen bond-based mechanism, underlining the predominance of this type of mechanism. Gelator solutions, therefore, share many physical characteristics with surfactant solutions (e.g., thermoresponsiveness, thixotropy, micellization, lyotropism, and crystallization) as well as with polymer solutions (e.g., swelling and microscopic mass motion).

Fluorinated liquids have also successfully been gelled using molecules that were themselves also fluorinated to some extent.^{17,18} George et al. showed that *N*-alkyl perfluoroalkanamides (F(CF₂)_{*m*}CONH(CH₂)_{*n*}H (denoted F_{*m*}NH_{*m*}) gelled a series of fluorinated liquids with varying degrees of success, with the gelation driven predominantly by the incompatibility of the fluorocarbon and hydrocarbon segments coupled with intermolecular hydrogen bonding. Previously, we reported the phase behavior of a homologous series of chiral, nonracemic *bis*-(α,β -dihydroxy ester)s found to gel mixtures of partially fluorinated liquids 2*H*,3*H*-perfluoropentane (HPFP) and 1*H*,1*H*-heptafluorobutanol (HFB).¹⁹ Thermoreversible gelation occurred and was shown to depend on both the solvent composition and the molecular structure of the gelator. The effects of chirality within the molecular structure have been previously noted for a wide

[†] Part of the Molecular and Polymer Gels; Materials with Self-Assembled Fibrillar Networks special issue.

*Corresponding author. E-mail: griffithspc@cardiff.ac.uk. Tel: +44 29 20875858. Fax +44 29 20874030.

(1) Gronwald, O.; Snip, E.; Shinkai, S. *Curr. Opin. Colloid Interface Sci.* **2002**, *7*, 148–156.

(2) Abdallah, D. J.; Weiss, R. G. *J. Braz. Chem. Soc.* **2000**, *11*, 209–218.

(3) Terech, P.; Weiss, R. G. *Chem. Rev.* **1997**, *97*, 3133–3159.

(4) Sangeetha, N. M.; Maitra, U. *Chem. Soc. Rev.* **2005**, *34*, 821–836.

(5) Smith, D. K. *Tetrahedron* **2007**, *63*, 7283–7284.

(6) Escuder, B.; Miravet, J. F. *Langmuir* **2006**, *22*, 7793–7797.

(7) Luboradzki, R.; Gronwald, O.; Ikeda, M.; Shinkai, S.; Reinhoudt, D. N. *Tetrahedron* **2000**, *56*, 9595–9599.

(8) Mieden-Gundert, G.; Klein, L.; Fischer, M.; Vogtle, F.; Heuze, K.; Pozzo, J. L.; Vallier, M.; Fages, F. *Angew. Chem., Int. Ed.* **2001**, *40*, 3164–3166.

(9) Weiss, R.; Terech, P., Eds.; *Molecular Gels: Materials with Self-Assembled Fibrillar Networks*; Springer: Dordrecht, The Netherlands, 2006.

(10) Yoza, K.; Ono, Y.; Yoshihara, K.; Akao, T.; Shinmori, H.; Takeuchi, M.; Shinkai, S.; Reinhoudt, D. N. *Chem. Commun.* **1998**, 907–908.

(11) Yoza, K.; Amanokura, N.; Ono, Y.; Akao, T.; Shinmori, H.; Takeuchi, M.; Shinkai, S.; Reinhoudt, D. N. *Chem.—Eur. J.* **1999**, *5*, 2722–2729.

(12) Hirst, A. R.; Smith, D. K. *Org. Biol. Chem.* **2004**, *2*, 2965–2971.

(13) Hirst, A. R.; Smith, D. K.; Feiters, M. C.; Geurts, H. P. M. *Chem.—Eur. J.* **2004**, *10*, 5901–5910.

(14) Hirst, A. R.; Smith, D. K.; Harrington, J. P. *Chem.—Eur. J.* **2005**, *11*, 6552–6559.

(15) Hirst, A. R.; Smith, D. K. *Chem.—Eur. J.* **2005**, *11*, 5496–5508.

(16) Burkhardt, M.; Kinzel, S.; Gradzielski, M. *J. Colloid Interface Sci.* **2009**, *331*, 514–521.

(17) George, M.; Snyder, S. L.; Terech, P.; Glinka, C. J.; Weiss, R. G. *J. Am. Chem. Soc.* **2003**, *125*, 10275–10283.

(18) George, M.; Snyder, S. L.; Terech, P.; Weiss, R. G. *Langmuir* **2005**, *21*, 9970–9977.

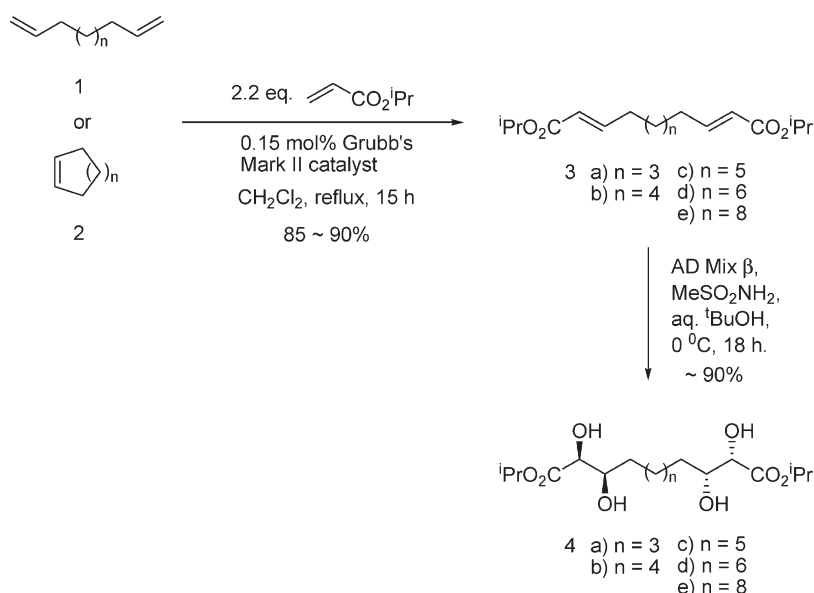
(19) Griffiths, P. C.; Cote, M.; James, R.; Rogueda, P. G.; Morgan, I. R.; Knight, D. W. *Chem. Commun.* **2005**, 3998–4000.

(20) Bao, C. Y.; Jin, M.; Lu, R.; Song, Z. G.; Yang, X. C.; Song, D. P.; Xu, T. H.; Liu, G. F.; Zhao, Y. Y. *Tetrahedron* **2007**, *63*, 7443–7448.

(21) Bag, B. G.; Maity, G. C.; Pramanik, S. R. *Supramol. Chem.* **2005**, *17*, 383–385.

(22) Brizard, A.; Oda, R.; Huc, I. In *Low Molecular Mass Gelators: Design, Self-Assembly, Function*; Fages F., Ed.; Springer: Berlin, 2005; Vol. 256, pp 167–218.

Scheme 1. Synthesis of Chiral Gelators



range of systems,^{11,20–35} especially in relation to amino acid-based molecules^{36–41} where chiral molecules act as gelators but racemic analogues do not. Generally, the molecular chirality determines the chirality of the macroscopic structure. In the case of the partially fluorinated solvents, the corresponding racemic *bis*-(α , β -dihydroxy ester)s did not form gels but rather precipitates,¹⁹ thus highlighting the important role of enantiomeric purity in such aggregation that also applies to fluorinated liquids. It is these observations that are elaborated here.

Materials and Methods

Materials. 2*H*,3*H*-Perfluoropentane (HPFP) (Apollo Scientific) was purified by filtration first through acidic and then basic alumina and then dried and stored over molecular sieves. 1*H*, 1*H*-Heptafluorobutanol (HFB) (Apollo Scientific) was stored

over molecular sieves but otherwise used as received. The solvent mixtures are expressed in terms of the mass fraction of HPFP, $\alpha_{\text{HPFP}} = m_{\text{HPFP}}/(m_{\text{HPFP}} + m_{\text{HFB}})$, where m_{HPFP} and m_{HFB} correspond to the masses of HPFP and HFB, respectively.

Synthesis of Gelators. The gelators were all synthesized in two high-yielding steps, either from a 1, ω -diene **1** or a cycloalkene **2**, depending upon commercial availability and the relative ease of preparation (Scheme 1).¹⁹ First, cross-metathesis with *iso*-propyl acrylate (many other alkyl acrylates were similarly employed) proceeded very smoothly and cleanly. Given that all components were scrupulously clean, this remarkable transformation could be completely catalyzed with only 0.15 mol % Grubb's Mark II catalyst and resulted in the isolation of diene diesters **3** in 85–90% yields solely as (E, E) isomers up to the limit of detection of both ¹H NMR and GC analysis.

Subsequent double *bis*-hydroxylation using AD Mix- β then delivered excellent yields of the expected tetrahydroxy diesters **4**. Chiral GC analysis of the derived trifluoroacetates, against a racemic dl mixture, showed the tetrahydroxy diesters **4** to be optically pure up to the limit of GC detection.

It should be noted that there is some potential for confusion among such structures depending upon the drawing style; this is illustrated in Scheme 2. Thus, a “full” drawing of the (2*S*,3*R*,12*R*,13*S*) enantiomer of organogelator **4e** in a standard “zigzag” form has all hydroxyls positioned on wedges, whereas an abbreviated representation, the right-hand structure, has the two pairs of hydroxyls on wedges and dashes; note also the alteration of the angle of the ester groups. Similar potential confusion arises with corresponding meso form **5** and is also shown in Scheme 2.

Nomenclature. The space length, n , of the gelator, denoted G_n , is defined as the number of carbons (methylene groups) between the two stereogenic centers (headgroups) less 2, in turn defined by the structure of the 1, ω -diene or a cycloalkene precursor, **1** or **2**.

Gel Formation. On a 1 g scale, the gelator was first dissolved in HFB, and the nonsolvent HPFP was subsequently added to give the desired composition. Gels prepared by adding the gelator directly to a predetermined solvent blend were found to be less reproducible. Rather unusually, no heating–cooling cycle was necessary for these gels, which form spontaneously at room temperature. The timescale for gel formation was found to differ according to the composition of the sample, ranging from a matter of seconds to a number of days. Here, only those gels that form over a period of an hour or less have been studied.

(23) Snijder, C. S.; deJong, J. C.; Meetsma, A.; vanBolhuis, F.; Feringa, B. L. *Chem.—Eur. J.* **1995**, *1*, 594–597.

(24) Haino, T.; Tanaka, M.; Fukazawa, Y. *Chem. Commun.* **2008**, 468–470.

(25) Babu, P.; Sangeetha, N. M.; Maitra, U. *Macromol. Symp.* **2006**, *241*, 60–67.

(26) Jung, J. H.; John, G.; Masuda, M.; Yoshida, K.; Shinkai, S.; Shimizu, T. *Langmuir* **2001**, *17*, 7229–7232.

(27) Hanabusa, K.; Maesaka, Y.; Kimura, M.; Shirai, H. *Tetrahedron Lett.* **1999**, *40*, 2385–2388.

(28) Mukkamala, R.; Weiss, R. G. *Langmuir* **1996**, *12*, 1474–1482.

(29) Watanabe, Y.; Miyasou, T.; Hayashi, M. *Org. Lett.* **2004**, *6*, 1547–1550.

(30) Hafkamp, R. J. H.; Feiters, M. C.; Nolte, R. J. M. *J. Org. Chem.* **1999**, *64*, 412–426.

(31) Sagawa, T.; Chowdhury, S.; Takafuji, M.; Ihara, H. *Macromol. Symp.* **2006**, *237*, 28–38.

(32) Sumiyoshi, T.; Nishimura, K.; Nakano, M.; Handa, T.; Miwa, Y.; Tomioka, K. *J. Am. Chem. Soc.* **2003**, *125*, 12137–12142.

(33) Becerril, J.; Burguete, M. I.; Escuder, B.; Galindo, F.; Gavara, R.; Miravet, J. F.; Luis, S. V.; Peris, G. *Chem.—Eur. J.* **2004**, *10*, 3879–3890.

(34) Tachibana, T.; Tomoko, M.; Kayako, H. *Bull. Chem. Soc. Jpn.* **1981**, *54*, 73–80.

(35) Tachibana, T.; Tomoko, M.; Kayako, H. *Bull. Chem. Soc. Jpn.* **1980**, *53*, 1714–1719.

(36) Doi, M.; Asano, A.; Yoshida, H.; Inouguchi, M.; Iwanaga, K.; Sasaki, M.; Katsuya, Y.; Taniguchi, T.; Yamamoto, D. *J. Pept. Res.* **2005**, *66*, 181–189.

(37) Caplar, V.; Zinic, M.; Pozzo, J. L.; Fages, F.; Mieden-Gundert, G.; Vogtle, F. *Eur. J. Org. Chem.* **2004**, 4048–4059.

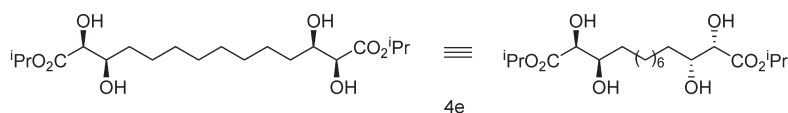
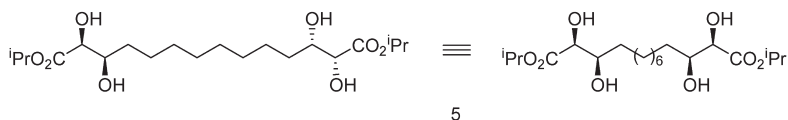
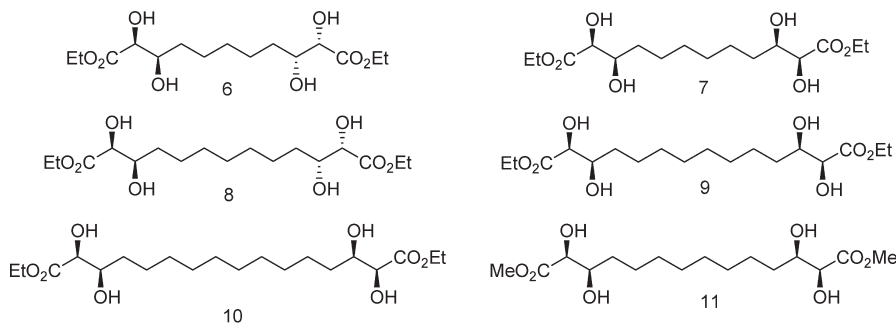
(38) Makarevic, J.; Jokic, M.; Raza, Z.; Stefanic, Z.; Kojic-Prodic, B.; Zinic, M. *Chem.—Eur. J.* **2003**, *9*, 5567–5580.

(39) Friggeri, A.; van der pol, C.; van Bommel, K. J. C.; Heeres, A.; Stuart, M. C. A.; Feringa, B. L.; van Esch, J. *Chem.—Eur. J.* **2005**, *11*, 5353–5361.

(40) Ihara, H.; Sakurai, T.; Yamada, T.; Hashimoto, T.; Takafuji, M.; Sagawa, T.; Hachisako, H. *Langmuir* **2002**, *18*, 7120–7123.

(41) Becerril, J.; Escuder, B.; Miravet, J. F.; Gavara, R.; Luis, S. V. *Eur. J. Org. Chem.* **2005**, 481–485.

Scheme 2. Stereochemical Representations of Chiral Gelators and Related Nongelators

A single (*S,R,R,S*) enantiomer, **4e**, of a *dl* pair.The related *meso* (*S,R,S,R*) form, **5**, in two contrasting stereodrawings.Molecules [**6** - **11**] identified in this work as being non- or poorly gelating

Determination of Gelation Temperature $T_{\text{gel-sol}}$. Glass vials containing the samples were equilibrated in a temperature-controlled water bath, and the temperature was increased from 15 °C initially in 2 °C steps with a 30 min equilibration time at each temperature. On approaching the gelation temperature, smaller increments (0.5 °C) were adopted. The simplest measure of gelation—that the gel be stable to inversion³—was used to quantify the gel–sol behavior because the volatile nature of the solvents rendered a rheological characterization unfeasible.

Small-Angle Neutron Scattering (SANS). Small-angle neutron scattering (SANS) measurements were performed on the fixed-geometry time-of-flight LOQ diffractometer (ISIS Spallation Neutron Source, Oxfordshire, U.K.). By using neutron wavelengths spanning 2.2 to 10 Å, a $Q = [4\pi \sin(\theta/2)]/\lambda$ range of approximately 0.008–0.25 Å⁻¹ (25 Hz) is accessible, with a fixed sample–detector distance of 4.1 m. The samples were contained in 2 -mm-path-length, UV-spectrophotometer-grade quartz cuvettes (Hellma) and mounted in aluminum holders on top of an enclosed, computer-controlled sample chamber. Sample volumes were approximately 0.4 cm³. Temperature control was achieved through the use of a thermostatted circulating bath pumping fluid through the base of the sample chamber. Under these conditions, a temperature stability of better than ±0.5 °C can be achieved. Experimental measuring times were approximately 40 min.

All scattering data were (a) normalized for the sample transmission, (b) background corrected using a quartz cell filled with the appropriate solvent (this also removes the inherent instrumental background arising from vacuum windows), and (c) corrected for the linearity and efficiency of the detector response using the instrument-specific software package. The data were put onto an absolute scale by reference to the scattering from a partially deuterated polystyrene blend.

The Kholodenko–Dirac wormlike chain model^{9,42} has been used to analyze the SANS data. This approach is derived from a Gaussian coil model where long, thin rods are made of a succession of m cylindrical elements of statistical length l and radius R_{ax}

The contour length of the chain, L , is equal to the product ml . The scattering intensity generated from Kholodenko–Dirac wormlike chains is proportional to two terms:

$$I(Q) \propto P_{\text{worm}}(Q) P_{\text{axial}}(Q) \quad (1)$$

The Kholodenko–Dirac model therefore smoothly interpolates between the Gaussian coil and rigid rod predictions and the number of segments (m) forming the chain and hence gives an indication regarding the flexibility of the chain. Smaller values of m correspond to stiffer chains. When m tends toward infinity, the scatterer adopts a flexible Gaussian random coil whereas when tending toward unity a rigid rod is obtained.

For long, thin rods

$$P_{\text{worm}}(Q) = \frac{2}{3m} \int_0^{3n} \left(1 - \frac{y}{3m}\right) f(y) dy \quad (2)$$

where for $Q \leq 3/l$, $f(y) = [\sinh(Ey)/E \sinh(y)]$ with $E = [1 - (Ql/3)^2]^{1/2}$ whereas for $Q > 3/l$, $f(y) = [\sin(Fy)/F \sinh(y)]$ with $F = [(Ql/3)^2 - 1]^{1/2}$, given that m is the number of chain elements, l is the statistical chain element length (giving a total chain length of $L = ml$).

$P_{\text{axial}}(Q)$ was adopted with a radial Guinier form, such as

$$P_{\text{axial}}(Q) = N(\rho_1 - \rho_3)^2 (AL)^2 \exp\left(-\frac{1}{2} Q^2 R_{\text{ax}}^2\right) \quad (3)$$

with ρ_1 and ρ_3 being the scattering-length densities for the worm and solvent, N being the worms per unit volume, A being the cross-sectional area, and R_{ax} being the cross-sectional radius of the chain, assuming a Gaussian scattering density.

CD Spectroscopy. Preformed gels prepared as described previously were transferred to the CD cells and either equilibrated at each set temperature for 20 min prior to recording the CD spectra or melted in situ and the gelation followed after a temperature jump. All spectra (180–400 nm) were recorded on a Chirascan instrument (Applied Photophysics).

(42) Kholodenko, A. L. *Macromolecules* **1993**, *26*, 4179–4183.

Results

1. Nongelling Structures. The inter-relationship between chirality and end-group structure plays an important role in determining the ability of this family of *bis*-(α,β -dihydroxy ester)s to gel mixtures of HPFP and HFB. Scheme 2 present nongelling structures 6–11, with nongelling being defined as materials that are either insoluble or show no gelation up to a concentration of 1 wt %. These very small changes in molecular structure reflect the surprisingly sensitive dependence on solubility—methyl- and ethyl-tipped analogues (Scheme 2) showing minimal solubility and no gelation ability whereas *iso*-butyl ($n = 2,6$), *tert*-butyl ($n = 6$), and *iso*-amyl ($n = 2$) are too soluble. *Isopropyl* possesses what seems to be the optimum structure for gelation over a wide range of chain lengths ($n = 1-3, 6$, and 8).

2. Thermodynamic Analysis of the Melting Transition $T_{\text{gel-sol}}$. As described by Murata et al.⁴³ and Terech et al.,⁴⁴ drawing on an analogy with the dissolution of crystals (Shröder–van Laar),⁴⁵ the enthalpy associated with the melting transition of the gelled networks can be evaluated via

$$\ln[G_n] = -\frac{\Delta H_m}{RT_m} + Cnst \quad (4)$$

where $[G_n]$ represents the concentration of gelator of size n and ΔH_m represents the phase-transition enthalpy. Figure 1a presents this analysis for gelators G_3, G_4, G_5, G_6 , and G_8 for $\alpha_{\text{HPFP}} = 0.9$ (i. e., 90/10 wt % HFPP/HFB solvent ratio) while Figure 1b reports $T_{\text{gel-sol}}$ for G_6 in a series of differing solvent ratios. Table 1 show the thus-determined enthalpies (ΔH_m) viz. G_3, G_4, G_5, G_6 , and G_8 for $\alpha_{\text{HPFP}} = 0.9$ and G_6 for $\alpha_{\text{HPFP}} = 0.95, 0.9, 0.85, 0.8$, and 0.7. First, all of these ΔH_m values are positive, showing that the melting process is endothermic, leading to a system with higher entropy. Second, these ΔH_m values are largely unaffected by the solvent composition or by the gelator chain length, suggesting that gelation is a feature dominated by the common structural motif, the end group. These enthalpy values are in good agreement with those reported in the literature for cholesterol,⁴³ 2-anthraquinonyl steroid,²⁸ anthracene,⁴⁴ 1-*O*-methyl-4,6-*O*-benzylidene derivatives,¹¹ and the dendritic aliphatic diamine systems⁴⁶ and much greater than that observed for HAS in ethylene glycol but smaller than that observed for van Gorp's C_3 -symmetric molecules.⁴⁷

3. Driving Force for Self-Assembly. The importance of the chirality in the gelation and the structure of the gelators lend themselves to a gelation mechanism based on hydrogen bonding. Accordingly, IR spectroscopy has been used to probe the nature of the hydrogen bonding occurring in these systems, and representative spectra are given in the Supporting Information.

The hydrogen bonding region shows a number of features that are dependent on the gelator concentration: sharp peaks around 3680 and 3640 cm^{-1} indicative of discrete H-bonds whereas the broad region arises from a collection of ill-defined H-bonds. On gelation, there is a noticeable shift in the band toward lower wavenumbers and a broadening of this band, indicating a small but distinguishable difference in the hydrogen bonding framework in the solution and the gel. One may envisage hydrogen

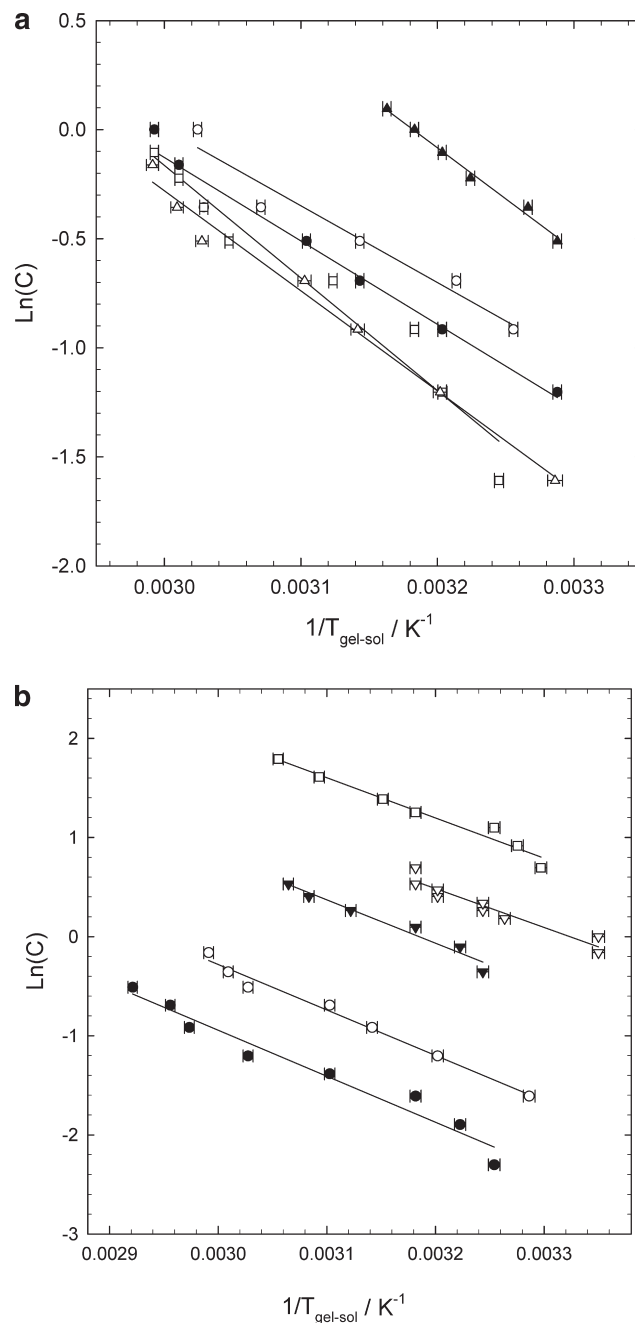


Figure 1. (a) Shröder–van Laar analysis of the gelation of a series of gelators with $n = 3$ (○), 4 (▲), 5 (●), 6 (△), and 8 (□) in $\alpha_{\text{HPFP}} = 0.9$. (b) Shröder–van Laar analysis of the gelation of gelator G_6 as a function of solvent composition, $\alpha_{\text{HPFP}} = 0.95$ (●), 0.90 (○), 0.85 (▼), 0.80 (▽), and 0.70 (□).

bonds between the hydrogen in the hydroxy group and the ester oxygen. This bonding could be either inter- or intramolecular, and it is theorized here that gelation induces a switch from intra- to intermolecular interactions.

4. Local Structure of the Aggregates. Circular dichroism (CD) spectroscopy measures the differences in absorption of left-handed and right-handed polarized light arising from structural asymmetry (chirality). Normally, the absence of regular structure results in no measurable CD intensity whereas an ordered structure results in a spectrum, but one that may exhibit both positive and negative intensity. Our previous observation that gelators of specific stereochemistry are required to form gels implies that the gelation mechanism requires a specific molecular

(43) Murata, K.; Aoki, M.; Suzuki, T.; Harada, T.; Kawabata, H.; Komori, T.; Ohseto, F.; Ueda, K.; Shinkai, S. *J. Am. Chem. Soc.* **1994**, *116*, 6664–6676.

(44) Terech, P.; Meerschaut, D.; Desvergne, J. P.; Colomes, M.; Bouas-Laurent, H. *J. Colloid Interface Sci.* **2003**, *261*, 441–450.

(45) Abdallah, D. J.; Weiss, R. G. *Langmuir* **2000**, *16*, 352–355.

(46) Lescanne, M.; Colin, A.; Mondain-Monval, O.; Fages, F.; Pozzo, J. L. *Langmuir* **2003**, *19*, 2013–2020.

(47) van Gorp, J. J.; Vekemans, J. A. J. M.; Meijer, E. W. *J. Am. Chem. Soc.* **2002**, *124*, 14759–14769.

Table 1. Phase-Transition Enthalpies ($\Delta H_m/kJ mol^{-1}$) for the Selection of Gelators and Fluorinated Solvent Mixtures Considered Here

HPFP/HFB mass ratio	gelator size, G_n				
	G_3	G_4	G_5	G_6	G_8
0.95				38 ± 2	
0.9	28 ± 2	38 ± 2	32 ± 2	32 ± 2	39 ± 2
0.85				36 ± 2	
0.8				34 ± 2	
0.7				34 ± 2	

arrangement. Rather interestingly, however, G_6 in $\alpha_{HPFP} = 0.9$ in the gelled state showed only a weak, ill-defined CD spectrum, but when the sample was melted, a strong CD spectrum was observed, contrary to the more common observation^{28,32,47,48} that the ordering introduced via gelation results in a strong CD spectrum.

The *bis*-(α,β -dihydroxy ester)s studied here contain a CD-active chromophore—the α -hydroxy ester moiety—that may exist in two possible conformations;⁴⁹ the preferred conformation (the carbonyl and alcohol distal) gives rise to a strong positive signal at 210 nm whereas the less favored conformation gives rise to a weaker negative signal at 230–240 nm. The shorter-wavelength CD signature—the strong positive signal from 210 to 220 nm—has also been associated with the formation of helical aggregates, when coincident with a negative signal at 201 nm.³²

Accordingly, a solution of 1 wt % G_6 in $\alpha_{HPFP} = 0.9$ was melted and transferred into a 1-mm-path-length quartz cell and was allowed to gel by holding the cell at 5 °C for 30 min. The temperature was then increased and the sample was equilibrated at each new temperature for 10 min before the CD spectrum was recorded (Figure 2a). An analogous experiment was also performed in which the gelation process was followed by recording the CD spectrum from a sample initially at 60 °C (i.e., in the liquid state) that had been placed into the sample stage thermostatted at 20 °C (Figure 2b).

Both of the expected signals—210 and 230–240 nm—are seen in Figure 2a,b, with the longer-wavelength signal (230 nm) appearing upon gelation because this signal arises from the less-preferred conformation of the α -hydroxy ester moiety; gelation imposes a conformational perturbation rather than being driven by such a conformational rearrangement.

5. Morphology of Gelled Systems. A series of samples made with gelator G_6 at concentrations of 0.4 wt % $< [G_6] < 0.8$ wt % in $\alpha_{HPFP} = 0.9$ were investigated by SANS at 25 °C, and the scattering data were interpreted in terms of the Kholodenko–Dirac wormlike chain (Figure 3a and Table 2).

The initial scattering intensity increases with the gelator concentration (Supporting Information, Figure 6S), showing that even though the size and shape of the scatterers was not found to vary significantly with concentration, the number of scatterers does increase, reflecting directly the increase in $T_{gel-sol}$ observed for increasing gelator concentration. The morphology of the gelled structure seems insensitive to gelator concentration and solvent composition, Figure 3a and Table 2, elaborated in the Supporting Information (Figures 5S and 7S; Tables 1S and 2S).

SANS was also used to explore the thermoreversibility of the gelation process. A sample of 0.7 wt % G_6 in $\alpha_{HPFP} = 0.9$ was examined as a function of temperature. Figure 3b presents the scattering data along with the Kholodenko–Dirac model fittings, and Table 2 presents the parameter values obtained. Again, the

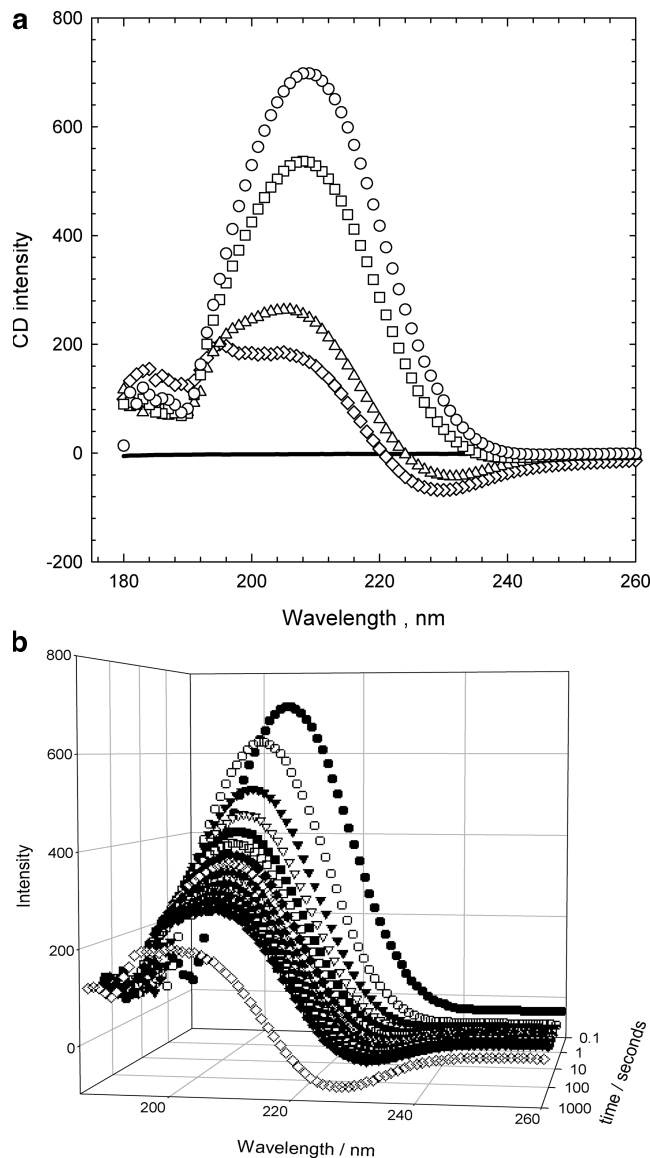


Figure 2. (a) CD spectrum for a 1 wt % solution of G_6 in $\alpha_{HPFP} = 0.9$ as function of temperature: 5 (◇), 25 (△), 45 (□), and 55 °C (○). Also shown is the absence of a CD spectrum from the solvent (—). (b) Loss of intensity of the CD spectrum for a 1 wt % solution of G_6 in $\alpha_{HPFP} = 0.9$ induced by gelation following a drop in temperature from 55 to 20 °C. Sixty CD spectra were recorded every 73 s, followed by an “infinite” spectrum recorded after a further delay of 12 h.

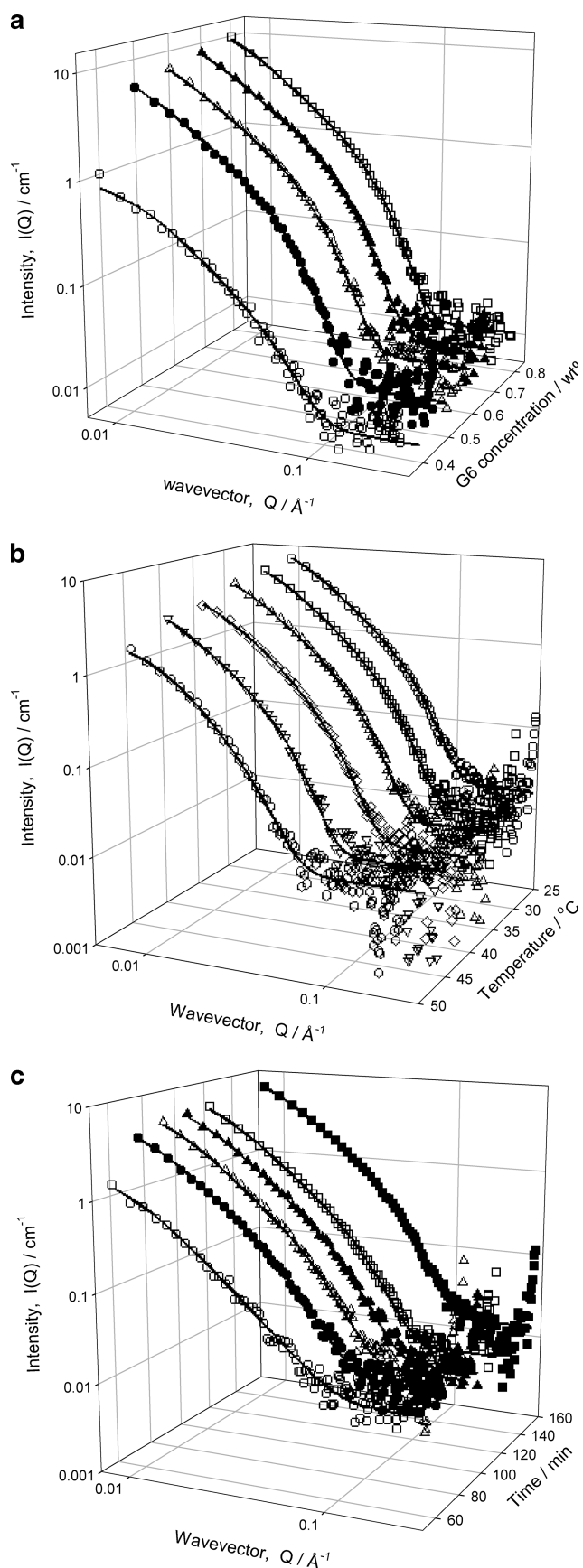
geometry of the scatterers appears to remain constant throughout the temperature range. The initial intensity varies linearly with temperature, and while the structure remains a gel at 50 °C ($T_{gel-sol} = 57 \pm 2$ °C), this decrease in initial intensity implies a loss of structural integrity. Furthermore, the rebuilding of the gelled structure was also investigated by heating a sample to ~ 70 °C (i.e., fully liquid), and the scattering was recorded once the sample was returned to 25 °C (Figure 3c).

Discussion

The IR spectra do not reveal any significant changes in hydrogen bonding upon melting of the gel, implying that if H-bonding is implicated in the gelation mechanism and is either responsible for or a reflection of the change in conformation around the ester it is likely to be a switch from intramolecular to intermolecular hydrogen bonding. A number of different

(48) Bao, C. Y.; Jin, M.; Lu, R.; Song, Z. G.; Yang, X. C.; Song, D. P.; Xu, T. H.; Liu, G. F.; Zhao, Y. Y. *Tetrahedron* **2007**, *63*, 7443–7448.

(49) Craig, J. C.; Pereira, W. E.; Halpern, B.; Westley, J. W. *Tetrahedron* **1971**, *27*, 1173–1184.



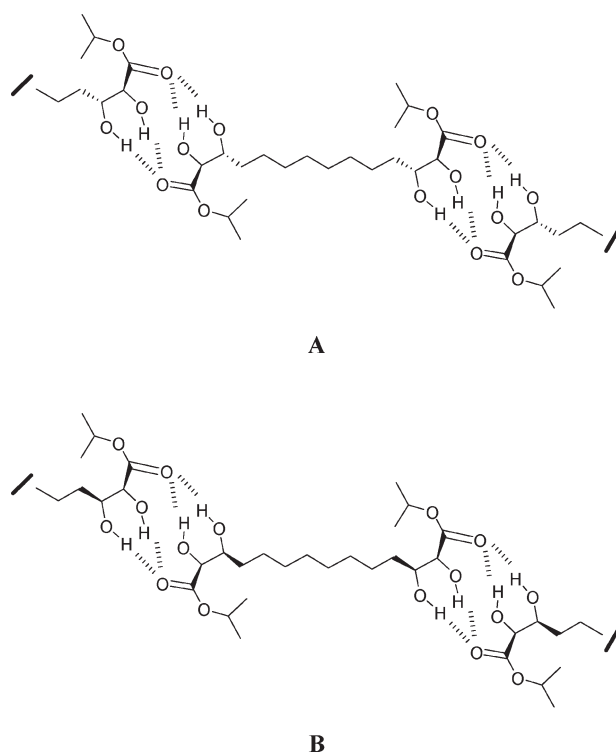
molecular arrangements may be envisaged consistent with four hydrogen bonds per headgroup and the conformation implied in the NMR experiment; one such arrangement is presented in

Figure 3. (a) SANS from gelator G_6 in $\alpha_{\text{HPFP}} = 0.9$ at concentrations of 0.4 (○), 0.5 (●), 0.6 (△), 0.7 (▲), and 0.8 wt % (□). The full lines are fits to the Kholodenko–Dirac model as described in the text. (b) SANS from 0.7 wt % gelator G_6 in $\alpha_{\text{HPFP}} = 0.9$ as a function of temperature: 25 (○), 30 (□), 35 (△), 40 (◇), 45 (▽), and 50 °C (○). The full lines are fits to the Kholodenko–Dirac model as described in the text. (c) SANS from 0.7 wt % gelator G_6 in $\alpha_{\text{HPFP}} = 0.9$ as a function of time after melting in situ: 50 (○), 65 min (●), 80 min (△), 95 min (▲), 110 min (□), endpoint (■). The full lines are fits to the Kholodenko–Dirac model as described in the text.

Table 2. Kholodenko–Dirac Model Fit Parameters for G_6 in $\alpha_{\text{HPFP}} = 0.9$ ($T = 25^\circ\text{C}$) as a Function of Gelator Concentration

[gelator]/wt %	$R_{\text{ax}} (\pm 2)/\text{Å}$	$m (\pm 0.5)$	$l (\pm 25)/\text{Å}$	$L = ml (\pm 20)/\text{Å}$
0.4	25	3.8	175	650
0.5	31	3.3	300	1000
0.6	32	3.0	350	1000
0.7	31	3.2	300	1000
0.8	30	4.3	250	1075

Scheme 3. Possible Intermolecular Hydrogen Bonding Structures That Drive Gelation^a



^a (A) Derived from gelator **4e**. (B) Less-favored cis-substituted structures derived from the meso form, which is a much less active gelator.

Scheme 3. This conformation promotes the exposure of the *iso*-propyl groups to the fluorinated media and parallels the increase in solubility observed for ethylene oxide polymers induced by methyl endgroups.^{50,51} Increases in the interheadgroup spacing, effectively $n + 2$ (Schemes 1 and 2), introduce sufficient flexibility into the molecule that in these cases the hydrogen bonding need not be predominantly intermolecular, thereby resulting in a reduced propensity for association, in turn leading to insolubility. Bulky headgroups (Scheme 2) introduce a steric barrier to

(50) Cote, M.; Rogueda, P. G. A.; Griffiths, P. C. *Int. J. Pharm.* **2008**, *362*, 147–152.

(51) Cote, M.; Rogueda, P. G. A.; Griffiths, P. C. *J. Pharm. Pharmacol.* **2008**, *60*, 593–599.

Table 3. Kholodenko–Dirac Model Fit Parameters for 0.7 wt % G₆ in α_{HFPF} = 0.9 as a Function of Temperature

temperature/°C	R _{ax} (±2)/Å	m (±0.5)	l (±25)/Å	L = ml (±20)/Å
25	31	3.2	300	1000
30	28	6.7	150	1000
35	30	4.8	200	1000
40	30	5.1	175	850
45	36	2.9	300	875
50	34	12.6	100	1250

efficient intermolecular hydrogen bonding; therefore, these molecules do not act as gelators. Similar conclusions were drawn by Samiyoshi et al.³² in their diamide system. From the enthalpy of melting values listed in Table 1, each cross-link in the gel network consists of approximately three to four hydrogen bonds, consistent with the molecular structure.

The most common macroscopic structural arrangement formed by (chiral) gelators consists of fibrils formed from the stacking of the gelator molecules.^{20,21,24,27,32,33,41,52–56} Compared to X-ray diffraction, there have been relatively few SANS studies of gelator systems, with most focusing either on “signature” intensity versus wave vector (Q) relationships, viz. Q^{-1} (rod) at low Q becoming Q^{-4} (solid objects) at higher Q in conjunction with local maxima or oscillations at higher Q arising from Bragg reflections or sharp interfaces, or the switch from a Q^{-1} to a Q^{-2} dependence in a double-logarithmic $I(Q)$ versus Q plot.^{17,57,57–60,60,61,61–65} There are no such features in the data presented here (Supporting Information, Figures 3S, 5S, and 7S); therefore, an alternative approach is required.

We have applied a more elaborate model of the above, treating the gelator morphology as a flexible assembly of rodlike structures. The balance between the flexibility and rigidity of the system is defined by parameter m . Here, there appears to be a rather consistent value of $m = 4.5(\pm 1.5)$, indicating a rather rigid structure, with a Gaussian cross-section of 31 ± 3 Å that is seemingly independent of solvent composition as well as gelator concentration and structure, consistent with that observed by van Gorp.⁴⁷ The axial radius (31 ± 3 Å for G₆, Tables 2 and 3) is comparable to the fully extended length of the gelator molecule, 28 Å, suggesting that the cross-section of the supramolecular structure comprises two gelators assembled in a head-to-tail arrangement via hydrogen bonding. Two additional gelator

molecules can then assemble above and below this pair, with the vertical structure determined by the registry of the hydrogen bonds and the headgroup chirality driving a twist leading to a “ribbon”. A mismatch in the registration of the hydrogen bonding would allow for the occurrence of some branching or fractal character. The Kuhn length of the rodlike segments is typically several hundred angstroms in size and reasonably constant except when the gel is not well-established (i.e., either at low gelator concentrations or temperatures close to the critical gel temperature). It should be stated, however, that dimensions of this magnitude are approaching the limit of what can be accurately measured on this SANS instrument and may account for the lack of a clear Q^{-1} signature at low Q . With an increase in temperature (or a decrease in concentration), the number density of these structures decreases whereas their size remains largely invariant until close to the critical gel temperature or concentration.

One may draw an analogy with polymer physics and calculate the parameter C^* , defined as the concentration at which adjacent polymer coils start to overlap. This concentration frequently coincides with an increase in the viscosity of the solution. For these gelators, taking the dimension L and assuming that the self-assembled structures sweep a spherical volume consistent with this dimension, the critical overlap concentration corresponds to a structure of some thousands of gelator molecules, which is not inconsistent with a stack of molecules of this size. Whereas this calculation is somewhat approximate, it does lend support to the proposed configuration. A more precise calculation would require detailed insight into the packing of the molecules, and future studies will address this issue.

Conclusions

It is shown here that chiral nonracemic *bis*-(α,β -dihydroxy ester)s are able to gel partially fluorinated solvents, a process proposed to be driven by hydrogen bonding. Racemic analogues did not act as gelators, exhibiting greatly reduced solubilities. The gelation ability was found to be sensitive to both endgroup structure and interheadgroup spacer length. These facets point to an association driven by intermolecular hydrogen bonding between the headgroups. The ability of the headgroups to participate in this process depends on the mutual accessibility of these headgroups; bulky headgroups and larger interheadgroup distances both preclude gelation. The macroscopic morphology was examined by SANS and interpreted in terms of a flexible arrangement of aggregated rods formed from a twisted stack of gelator molecules.

Acknowledgment. EPSRC, Cardiff University, and AstraZeneca are gratefully thanked for the provision of studentships (M.C. and I.R.M.), and STFC is acknowledged for access to neutron facilities.

Supporting Information Available: Further analysis and interpretation of the SANS data presented here (Kratky plots, Q^{-1} to Q^{-2} crossover analysis plus evidence to show that there is no structure factor $S(Q)$ in the data), supported by additional SANS data pertaining to a wider range of solvent composition and gelator structure, along with IR and NMR analyses. This material is available free of charge via the Internet at <http://pubs.acs.org>.

(52) Fu, X. J.; Yang, Y.; Wang, N. X.; Wang, H.; Yang, Y. *J. Mol. Recognit.* **2007**, *20*, 238–244.

(53) Das, D.; Dasgupta, A.; Roy, S.; Mitra, R. N.; Debnath, S.; Das, P. K. *Chem.—Eur. J.* **2006**, *12*, 5068–5074.

(54) Smith, J. M.; Katsoulis, D. E. *J. Mater. Chem.* **1995**, *5*, 1899–1903.

(55) Pantos, G. D.; Pengo, P.; Sanders, J. K. M. *Angew. Chem., Int. Ed.* **2007**, *46*, 194–197.

(56) Zhan, C. L.; Gao, P.; Liu, M. H. *Chem. Commun.* **2005**, 462–464.

(57) George, M.; Funkhouser, G. P.; Terech, P.; Weiss, R. G. *Langmuir* **2006**, *22*, 7885–7893.

(58) Okabe, S.; Ando, K.; Hanabusa, K.; Shibayama, M. *J. Polym. Sci., Part B: Polym. Phys.* **2004**, *42*, 1841–1848.

(59) Okabe, S.; Hanabusa, K.; Shibayama, M. *J. Polym. Sci., Part B: Polym. Phys.* **2005**, *43*, 3567–3574.

(60) Terech, P.; Bouaslaurent, H.; Desvergne, J. P. *J. Colloid Interface Sci.* **1995**, *174*, 258–263.

(61) Terech, P.; Clavier, G.; Bouas-Laurent, H.; Desvergne, J. P.; Deme, B.; Pozzo, J. L. *J. Colloid Interface Sci.* **2006**, *302*, 633–642.

(62) Dastidar, P.; Okabe, S.; Nakano, K.; Iida, K.; Miyata, M.; Tohnai, N.; Shibayama, M. *Chem. Mater.* **2005**, *17*, 741–748.

(63) Terech, P.; Furman, I.; Weiss, R. G. *J. Phys. Chem.* **1995**, *99*, 9558–9566.

(64) Terech, P.; Allegraud, J. J.; Garner, C. M. *Langmuir* **1998**, *14*, 3991–3998.

(65) Willemsen, H. M.; Marcelis, A. T. M.; Sudholter, E. J. R.; Bouwman, W. G.; Deme, B.; Terech, P. *Langmuir* **2004**, *20*, 2075–2080.